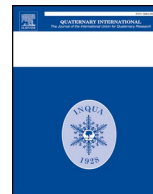




ELSEVIER

Contents lists available at ScienceDirect

Quaternary International

journal homepage: www.elsevier.com/locate/quaint

Trace metal analysis of sediment cores using a novel X-ray fluorescence core scanning method

Rick Hennekam^{a,*}, Tim Sweere^{a,b}, Rik Tjallingii^c, Gert J. de Lange^b, Gert-Jan Reichart^{a,b}^a NIOZ Royal Netherlands Institute for Sea Research, Department of Ocean Systems, and Utrecht University, P.O. Box 59, 1790 AB, Den Burg, Texel, the Netherlands^b Department of Earth Sciences, Faculty of Geosciences, Utrecht University, P.O. Box 80.121, 3508 TA, Utrecht, the Netherlands^c GFZ German Research Centre for Geosciences, Section 5.2 – Climate Dynamics and Landscape Evolution, Potsdam, Germany

ARTICLE INFO

Keywords:

Trace metals
XRF core scanning
High-resolution geochemistry
Paleoclimate
Paleoenvironment

ABSTRACT

The trace-metal composition of sediments provides important information on (past) environmental conditions, such as bottom water oxygenation, marine productivity, sediment provenance, and pollution. Whereas major and minor elements are often routinely analyzed using X-Ray Fluorescence (XRF) core scanning, analysis of trace metals with the same method is not yet established as a routine procedure. Here, we used a recently developed state-of-the-art XRF detector with a core scanner (Avaatech) to examine the optimal settings for analyzing a suite of trace metals (V, Cr, Ni, Cu, Zn, Mo, and U). Settings were optimized for fast analyses of sediment cores by extensive testing of primary energy settings, filters, and exposure times on two eastern Mediterranean Sea sapropel layers that archive episodes of past sea-floor anoxia. We reveal the following most advantageous (i.e., optimized for analytical accuracy and time efficiency) settings: (1) V, Cr, Ni at 20 kV with aluminum primary beam filter, (2) Cu, Zn, and U at 30 kV with ‘thick’ (125 μm) palladium primary beam filter, and (3) Mo at 50 kV with copper primary beam filter. For these trace elements, generally, ≥ 30 s of measurement are required for obtaining reliable data. Synthetic mixtures show that matrix effects, which are inherent to XRF analyses, are of particular importance for V. A correction for these matrix effects on V (e.g., using Compton scattering) may be necessary for samples with a large variability in carbonate content. XRF core-scanning measurements on synthetically laminated sediments show that trace metals with contrasting atomic weights and related XRF penetration depths (V and Mo) can be determined at sub-mm resolution. We show that intensity results from the new XRF detector can be converted into concentrations using multivariate log-ratio calibration, allowing a fast quantitative prediction of sedimentary trace metal content using XRF core scanning.

1. Introduction

The concentrations of trace metals in sedimentary archives provide important constraints on past environmental conditions. For instance, sedimentary concentrations of vanadium (V), chromium (Cr), molybdenum (Mo), and uranium (U), record past oxygenation of the oceans, because their solubility is related to the redox state (Algeo and Lyons, 2006; Brumsack, 2006; Tribovillard et al., 2006, 2012; Algeo and Tribovillard, 2009; Algeo and Rowe, 2012; Sweere et al., 2016). The sedimentary distribution for trace metals such as nickel (Ni), copper (Cu), and zinc (Zn) can also be associated to organic-matter sinking rate in the water column, potentially delivering information on export productivity (Bruland, 1980; Brumsack, 2006; Tribovillard et al., 2006). Moreover, trace metals are useful for sediment provenance discrimination (Garver et al., 1996; Yang et al., 2003), and detection of

sediment pollution (Ruiz, 2001). Conventional analyses of trace metals in sediments involve total destruction with strong acids followed by, e.g., Inductively Coupled Plasma-Mass Spectrometry (ICP-MS) analyses, or glass-bead preparation followed by off-line X-Ray Fluorescence (XRF) analyses. Although these methods are well established, they are also time consuming and costly. To address this issue, the use of XRF core scanning to determine sedimentary trace metal profiles is explored here.

XRF core scanning (XCS) is renowned for fast and high-resolution (up to < mm) sediment measurements, with relatively little cost (Croudace and Rothwell, 2015). Studies using XCS usually focus on major and minor elements, but trace metals such as Mo have also been analyzed (Wirth et al., 2013; Gibson and Peterson, 2014). Nonetheless, especially combinations of multiple trace metals provide powerful paleo-environmental proxies, such as the covariation of V, Mo, and U

* Corresponding author.

E-mail addresses: rickhennekam@gmail.com, rick.hennekam@nioz.nl (R. Hennekam).<https://doi.org/10.1016/j.quaint.2018.10.018>

Received 30 March 2018; Received in revised form 28 August 2018; Accepted 16 October 2018

Available online 25 October 2018

1040-6182/ © 2018 Elsevier Ltd and INQUA. All rights reserved.

Table 1

Results of the XCS settings test for trace element analysis performed on 14 Mediterranean sapropel samples from core MS21PC and 8 standards samples (the latter are only included in the right part of the table). A stepwise increase in energy (5 kV per step) and different filters (no filter, Al-, Pd-thin-, Pd-thick-, and Cu-filter) were used, all measured in triplicate with a measurement time of 10 s. Shown are the coefficient of determination (R^2) values for linear regressions of element counts from XCS measurements to element concentrations obtained through conventional methods. The concentration ranges of the elements are indicated in the top row. Color coding highlights R^2 values, i.e., red to green is 0.00–1.00 respectively (see color legend). Blue highlighted settings (left column) were used for further analyses to determine precision and most efficient measurement times.

Settings (Energy; Filter; Current)	excluding standards							including standards							Color legend R^2
	V (124-275 ppm)	Cr (97-127 ppm)	Ni (63-104 ppm)	Cu (54-77 ppm)	Zn (89-137 ppm)	Mo (0-67 ppm)	U* (2-10 ppm)	V (10-275 ppm)	Cr (10-137 ppm)	Ni (7-104 ppm)	Cu (13-426 ppm)	Zn (10-395 ppm)	Mo (0-67 ppm)	U* (1-14 ppm)	
10 kV; No filter; 400 μ A	0.78	-0.04	0.07	0.02	-0.49			0.89	0.64	-0.27	0.19	0.00			0.00
10 kV; Al filter; 1200 μ A	0.76	0.26	0.18	0.02	-0.10			0.89	0.86	0.01	0.41	0.11			0.10
15 kV; No filter; 125 μ A	0.80	0.06	0.39	0.00	-0.54			0.90	0.74	0.05	0.58	0.04		0.11	0.20
15 kV; Al filter; 600 μ A	0.88	0.43	0.51	0.34	-0.33		-0.01	0.91	0.91	0.72	0.97	0.54		0.11	0.30
20 kV; No filter; 75 μ A	0.84	0.36	0.40	0.09	-0.47	-0.04	0.00	0.90	0.81	0.32	0.77	0.18	-0.01	0.00	0.40
20 kV; Al filter; 250 μ A	0.85	0.50	0.67	0.11	-0.06	-0.02	-0.05	0.92	0.93	0.79	0.97	0.68	-0.04	-0.01	0.50
20 kV; Pd-thin filter; 1200 μ A	0.68	0.42	0.55	0.71	0.65	0.07	-0.03	0.87	0.92	0.83	0.98	0.92	0.11	-0.06	0.60
25 kV; No filter; 50 μ A	0.81	0.48	0.48	0.01	-0.48	0.14	0.00	0.88	0.81	0.32	0.88	0.29	0.11	-0.03	0.70
25 kV; Al filter; 140 μ A	0.77	0.35	0.57	0.49	0.00	0.15	-0.01	0.89	0.92	0.77	0.98	0.77	0.09	-0.03	0.80
25 kV; Pd-thin filter; 250 μ A	0.72	0.31	0.55	0.57	0.60	0.67	-0.02	0.89	0.88	0.72	0.98	0.92	0.62	-0.07	0.90
30 kV; No filter; 35 μ A	0.78	0.16	0.37	0.03	-0.38	0.42	-0.03	0.88	0.84	0.48	0.89	0.43	0.37	-0.08	1.00
30 kV; Al filter; 85 μ A	0.80	0.36	0.56	0.46	0.12	0.45	0.00	0.90	0.91	0.73	0.98	0.82	0.37	-0.12	
30 kV; Pd-thin filter; 200 μ A	0.62	0.15	0.47	0.69	0.74	0.76	0.02	0.84	0.85	0.68	0.98	0.93	0.74	0.00	
30 kV; Pd-thick filter; 1200 μ A	0.51	0.30	0.30	0.43	0.52	0.81	0.25	0.74	0.66	0.40	0.98	0.94	0.81	0.18	
30 kV; Cu filter; 1200 μ A	0.68	0.37	0.36	0.14	0.00	0.93	0.49	0.86	0.72	0.39	0.76	0.63	0.93	0.46	
35 kV; No filter; 30 μ A	0.81	0.13	0.44	0.17	-0.38	0.59	0.00	0.90	0.82	0.49	0.91	0.49	0.58	-0.08	
35 kV; Al filter; 50 μ A	0.75	0.36	0.53	0.37	0.28	0.69	0.09	0.89	0.88	0.71	0.97	0.88	0.66	0.03	
35 kV; Pd-thin filter; 100 μ A	0.58	0.06	0.39	0.39	0.70	0.70	0.03	0.80	0.77	0.61	0.98	0.93	0.65	0.01	
35 kV; Pd-thick filter; 1000 μ A	0.66	0.19	0.19	0.48	0.74	0.90	0.33	0.83	0.75	0.46	0.98	0.94	0.88	0.17	
35 kV; Cu filter; 800 μ A	0.53	0.08	0.18	0.17	0.00	0.95	0.63	0.79	0.68	0.21	0.90	0.79	0.95	0.49	
40 kV; No filter; 23 μ A	0.69	0.41	0.50	0.22	-0.25	0.68	0.00	0.87	0.87	0.55	0.91	0.59	0.62	-0.08	
40 kV; Al filter; 35 μ A	0.79	0.28	0.50	0.45	0.25	0.70	-0.01	0.89	0.83	0.66	0.97	0.88	0.70	-0.04	
40 kV; Pd-thin filter; 50 μ A	0.58	0.08	0.44	0.44	0.71	0.71	0.00	0.84	0.75	0.59	0.98	0.93	0.71	0.00	
40 kV; Pd-thick filter; 750 μ A	0.62	0.10	0.38	0.51	0.70	0.88	0.40	0.84	0.74	0.38	0.98	0.94	0.87	0.29	
40 kV; Cu filter; 400 μ A	0.53	0.08	0.29	0.26	0.04	0.96	0.40	0.78	0.68	0.12	0.93	0.83	0.96	0.38	
45 kV; No filter; 15 μ A	0.78	0.21	0.40	0.20	-0.03	0.72	0.00	0.90	0.82	0.50	0.93	0.76	0.63	-0.03	
45 kV; Al filter; 20 μ A	0.76	0.29	0.54	0.51	0.60	0.65	0.06	0.89	0.85	0.65	0.97	0.92	0.63	0.01	
45 kV; Pd-thin filter; 35 μ A	0.45	0.14	0.42	0.42	0.63	0.76	0.02	0.78	0.70	0.59	0.98	0.93	0.75	0.01	
45 kV; Pd-thick filter; 500 μ A	0.52	0.10	0.32	0.47	0.72	0.92	0.10	0.77	0.72	0.46	0.98	0.94	0.90	0.24	
45 kV; Cu filter; 200 μ A	0.38	0.28	0.27	0.15	0.12	0.96	0.60	0.64	0.46	0.12	0.93	0.90	0.95	0.52	
50 kV; No filter; 10 μ A	0.66	0.22	0.42	0.23	0.01	0.68	0.01	0.85	0.78	0.60	0.93	0.83	0.62	0.00	
50 kV; Al filter; 15 μ A	0.75	0.14	0.48	0.19	0.58	0.62	0.02	0.90	0.81	0.66	0.97	0.93	0.60	0.06	
50 kV; Pd-thin filter; 30 μ A	0.49	0.40	0.45	0.39	0.69	0.79	0.04	0.75	0.70	0.44	0.98	0.96	0.76	0.07	
50 kV; Pd-thick filter; 300 μ A	0.50	0.03	0.22	0.19	0.63	0.89	0.32	0.74	0.61	0.32	0.98	0.93	0.86	0.29	
50 kV; Cu filter; 100 μ A	0.24	0.19	0.10	0.24	0.31	0.94	0.33	0.50	0.25	0.03	0.94	0.94	0.94	0.24	

(Algeo and Tribouillard, 2009; Tribouillard et al., 2012), and, currently, these trace metals are not routinely measured by XCS. State-of-the-art digital silicon drift detectors, with increased detection speed and improved spectral resolution (~125 eV at Mn-K α), have recently become available and are potentially capable of in-situ trace-metal analyses on sediment surfaces using XCS. Here, we investigate the suitability of these new XRF detectors and describe the optimal methodology for trace metal analyses.

We present a systematic study aimed at establishing trace metal analyses using XCS, for which we use 4 consecutive steps. 1.) The optimal instrumental settings for trace element analyses are investigated. Specifically, we extensively test different combinations of X-Ray tube-energy settings, primary-beam filters, and analytical dwell times for 22 samples with known compositions. 2.) Optimized XCS settings for trace-metal analyses are applied to long sediment core records with known trace-metal distributions from the eastern Mediterranean Sea. The sedimentary sequence used contains two past intervals of basin-wide anoxia and enhanced organic-matter deposition (i.e., sapropels, see Rohling et al., 2015). Analyses are performed on wet core material and on dry powdered samples, to study the effects of interstitial water that can alter XCS measurements (Tjallingii et al., 2007; Hennekam and De Lange, 2012). The XCS data are converted to concentrations using a multivariate log-ratio calibration approach (Weltje et al., 2015) to evaluate XCS as a tool to perform fast quantitative geochemical

predictions. 3.) XCS measurements are performed on artificially produced laminations with set variable V and Mo concentrations, to deduce the potential effects of sub-mm-scale XRF scanning on elements of contrasting atomic weights. 4.) Sediment samples of three common matrices (i.e., quartz, clay, and calcite) were spiked with known amounts of trace metals and used to assess potential matrix effects for V and Mo. The focus is on V, as its K-line energies are in the middle of a wide range of major elements (K, Ca, Ti, Mn, Fe), which generally cause the strongest matrix effects (Croudace and Gilligan, 1990).

Optimal XCS settings for trace metal analyses established in this study are also considered for a wider range of detectors. For this, we performed tests on a larger range of concentrations with an earlier generation detector (resolution of ~180eV at Mn-K α), which we present in the Supplementary Material. These results are used to show that even with the older generation detector trace elements can be detected, albeit for higher concentrations, as long as sufficient count time and proper energy settings are used.

2. Material and methods

2.1. XRF core scanner, sample preparation, and reference standards

All the XCS analyses were acquired using an Avaatech core scanner at the Royal Netherlands Institute for Sea Research (NIOZ). This XRF

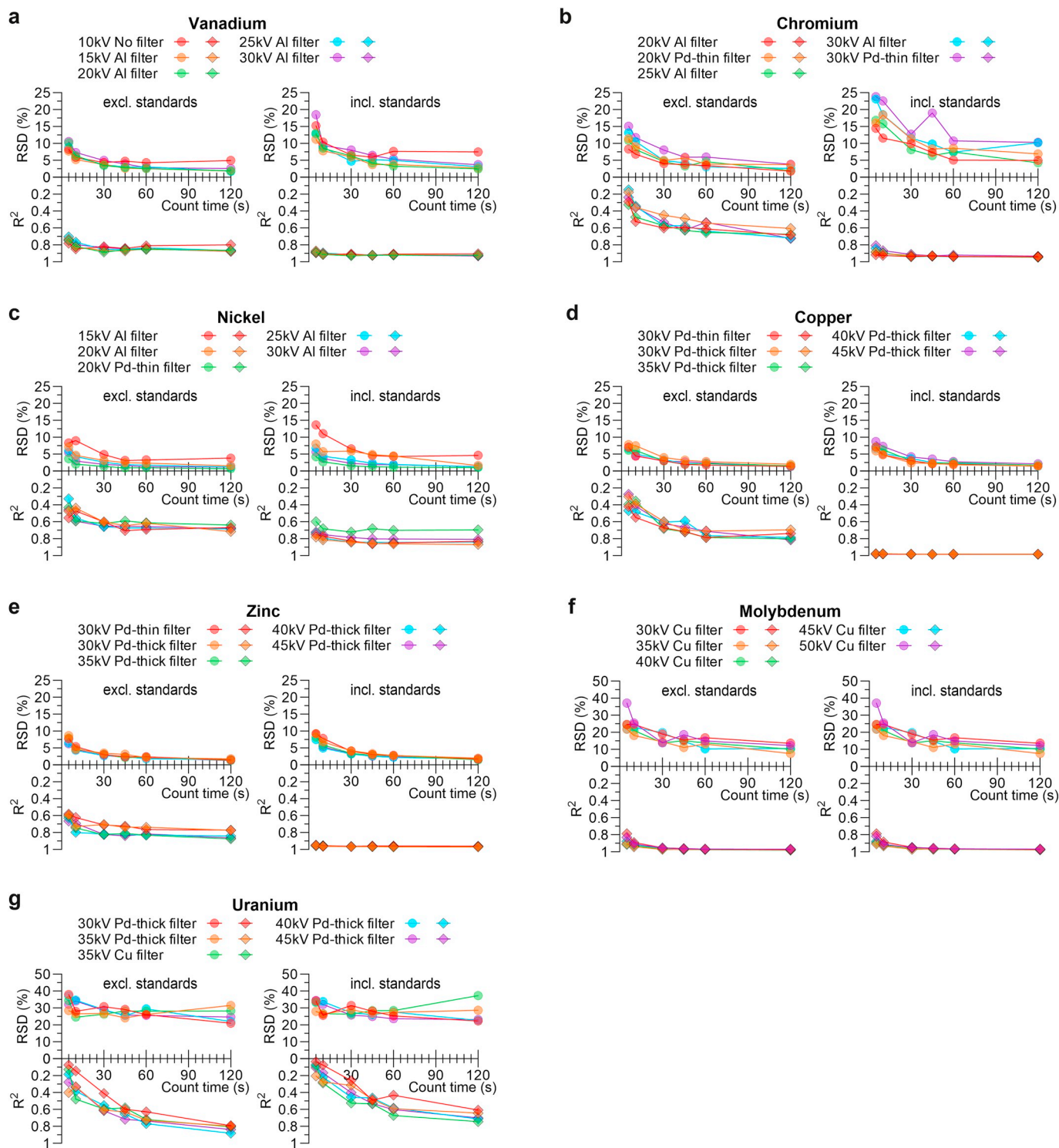


Fig. 1. XCS measurement time (5s, 10s, 30s, 45s, 60s, and 120s; X-axis) versus RSD (upper Y-axis) and coefficient of determination (R^2 ; lower Y-axis). The former are average RSD values combined from all samples, and the latter are determined through regression to concentration values from ICP-OES/ICP-MS measurements. The information for only the five settings that showed the best results (highest R^2) for a trace element are shown (see legends for those specific settings per element). The figure shows the trace elements: (a) V, (b) Cr, (c) Ni, (d) Cu, (e) Zn, (f) Mo, and (g) U. The left panels are for XCS measurements performed on 14 Mediterranean sapropel samples from core MS21PC only, while the right panels also included 8 standard samples. For Mo we only included the samples with Mo concentrations ≥ 10 ppm to calculate the RSD's, as the samples with lower concentrations were shown to be under the detection limit (see Section 3.1 and Fig. 2).

scanner is equipped with a 100W rhodium (Rh) X-Ray tube and with a Rayspec cubed SiriusSD silicon drift detector with a 40 mm² active area of which 30 mm² collimated. The detector contains a low capacity preamplifier integrated on the detector crystal, which allows an improved spectral resolution at short peaking times compared to older

generation detectors. The tube energy settings (1–50 kV at a maximum of 2 mA), primary beam filters (Aluminium (Al), Palladium (Pd) ‘thin’ (25 μ m), Pd ‘thick’ (125 μ m), and Cu), and measurement times were varied to obtain the optimal settings for trace element analyses. The electric current of the X-Ray source (0–2 mA) was selected to maintain a

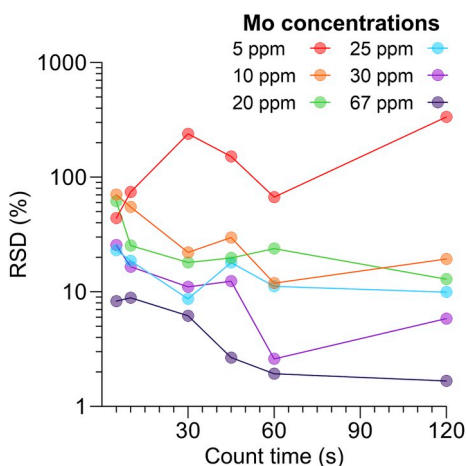


Fig. 2. RSD's of Mo (measured at 50 kV with a Cu filter) for different sample concentrations. RSD's of XCS measurements of samples with concentrations < 10 ppm remain high at all measurement times.

detector throughput with ~20–40% dead time (i.e., the time the detector is irresponsive while processing an X-Ray pulse) to minimize sum peak development with relatively high count rates. All the spectral data were processed using bAxil spectrum analysis software, which is developed by Brightspec.

The XRF analyses were performed on wet (“wet-XCS”) and dry (“dry-XCS”) sediment samples, with a 10 × 10 mm slit size. The wet sample measurements were acquired directly on the split core surfaces after covering the surface with a 4- μ m SPEXCerti Ultralene foil, which prevents dehydration of the sediment and avoids contamination of the measurement prism. Dry sample measurements were performed on freeze dried, thoroughly ground, sediment samples. Polyethylene containers with a circular opening of 15 mm width and 1.5 mm depth were filled with approximately 257 ± 28 mg (1 σ ; N = 79) of material and covered with 4- μ m SPEXCerti Ultralene foil.

For consistency control we measured eight external reference standards (GSR-4, GSR-6, GSD-10, JSd-1, JSd-3, MESS 3, SARM 2, and SARM 3), hand pressed in polyethylene containers, before and after every run of XCS measurements (i.e., a core section or a set of 58 polyethylene containers). For these standards we specifically monitored the light elements Al, Ca, and V, as these are potentially most affected by aging of the detector or variability in helium in the measurement triangle. We tested if the slope (sensitivity) and R^2 (accuracy) values of the regressions (X-Y cross-plots of concentration versus XCS intensities) for Al, Ca, and V were reproducible. Throughout all analyses the slope of the X-Y plot of the reference concentrations to XCS intensities of light elements Al, Ca, and V, varied less than 5%, while the R^2 varied less than 3% for these elements. Repeated analysis throughout the measurement series (N = 13) showed a precision (relative standard deviation) of < 2% for Al and Ca, and < 7% for V. This implies that the analytical setup and performance of the detector remained stable during the entire duration of the experiment. The determination of precision and accuracy for the XCS measurements are discussed in more detail in Section 2.4.

2.2. Mediterranean sediment material to test optimal trace metal method

Samples from an eastern Mediterranean Sea core (MS21PC; 32°20.7'N, 31°39.0'E; 1022 m water depth) (Hennekam et al., 2015; Rohling et al., 2017; Zwiep et al., 2018) were used to determine and test the optimal settings for trace metal analyses. Total core length is 751.5 cm, but this study focuses only on the top 1.5 m and bottom 2 m of the core, containing sapropel layers S1 (35–95 cm) and S3 (605–660 cm), respectively. These sapropels correspond to well-known intervals of eastern Mediterranean Sea deep-water anoxia (e.g., Rohling

et al., 2015). The reference half of the core sections was used for “wet” XCS analyses, while the working half was discretely sampled in 0.5-cm intervals. The discrete samples were measured by ICP-optical emission spectroscopy (ICP-OES) and partially by ICP-MS (approximately every 2-cm intervals, focused around both sapropels) (Hennekam et al., 2015; Zwiep et al., 2018). The same discrete samples from the working half of the core were also used for “dry” XCS measurements.

Before the ICP-OES and ICP-MS measurements, the samples (~125 mg) were totally digested using a procedure with HF-HClO₄-HNO₃ acid mixtures (details in Hennekam et al., 2015). The ICP-OES measurements were performed with a Spectro Ciros Vision ICP-OES at Utrecht University. Reference samples (ISE921) indicated a precision and accuracy (relative standard deviation; deviation from reference value) for the ICP-OES measurements: V (3%; ± 1%), Cr (4%; ± 4%), Ni(3%; ± 4%), Cu(3%; ± 8%), Zn (4%; ± 2%), and Mo (13%; not available). The ICP-MS measurements were performed with a Thermo Scientific X-Series 2 ICP-MS at Utrecht University. Reference samples (ISE921) indicated a precision and accuracy (relative standard deviation; deviation from reference value) for the ICP-MS measurements: Mo (3%; not available) and U (2%; ± 7%). No reference value is available for Mo in the ISE921 standard, but Mo measurements performed with both ICP-OES and ICP-OES methods showed an average deviation < 13% between the methods.

2.3. Testing XCS settings for trace metal analysis

To determine the optimal settings for trace metal analysis by XCS we first focused on 14 samples from the eastern Mediterranean Sea core MS21PC (34, 39, 50, 67, 84, 89, 120, 610, 614, 630, 655, 656, 659, and 680 cm depth in the core), which covered a range in concentrations for our target elements (ranges are shown at the top in Table 1). Ground, homogenized, dry sediment samples were used to avoid the impact of physical properties, such as water content, grain size, surface roughness, and surface slope, potentially biasing XCS results (Tjallingii et al., 2007; Hennekam and De Lange, 2012; Jarvis et al., 2015). Additionally, 8 reference standards (Section 2.1) were included in order to extend the trace-metal concentration range for these tests (see Table 1). The more variable composition of the reference standards may introduce some additional deviations due to matrix effects that are inherent to XRF. Therefore, we present data including and excluding these reference standards (Table 1; Fig. 1).

The 14 samples from the eastern Mediterranean Sea and the 8 reference standards were measured with variable tube energy settings, primary beam filters, and measurement times. At first, the XCS measurements were performed with a constant measurement time (10 s) and changing the energy settings of the Rh tube between 10 and 50 kV in steps of 5 kV. The primary beam filters (i.e., Al-, Pd-thin-, Pd-thick-, and Cu-filters) were used on all energy settings to reduce the spectral background. This resulted in a set of 35 different XCS settings that were used to analyze the 22 sediment samples in threefold. Based on the results of this test, we selected the settings that showed the most promising results for trace element analysis (i.e., highest R^2 with the traditional discrete sample analyses, see Section 2.4). Subsequently, we examined precision and accuracy of the XCS measurements for different measurement times applied. This was achieved through varying the dwell time (5, 10, 30, 45, 60, and 120 s) at all the selected energy/filter settings, while analyzing the 22 sediment samples in fivefold.

2.4. XCS data precision, accuracy, and calibration

The XCS data is initially presented as intensity rates (counts per second; cps), and after evaluation of the optimal settings, the XCS data were converted to concentrations (ppm) using the multivariate log-ratio calibration (MLC) model (Weltje et al., 2015). The optimal settings were evaluated by the optimal count statistics of the intensity records in terms of precision and accuracy. Precision was determined by

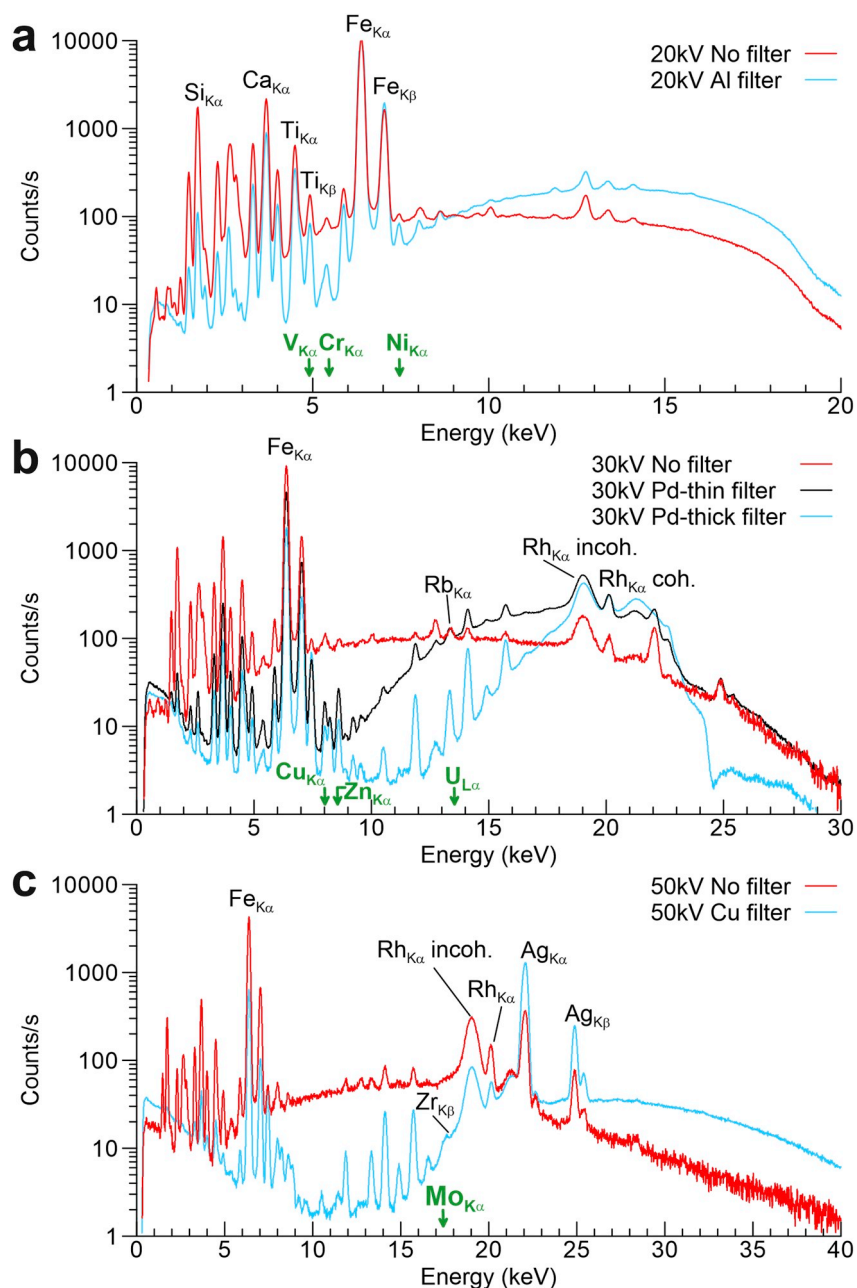


Fig. 3. XRF spectra from scans of a Mediterranean sediment sample (655 cm in core MS21), using settings at 20, 30, and 50 kV without and with primary beam filters (Al, Pd-thin, Pd-thick, and Cu filters).

Table 2
Instrumental settings ('optimal') used for specific sets of trace elements.

Tube voltage (kV)	Filter	Trace elements analysed	Currents used for Mediterranean sediments (dry; wet) (μA) ^a
20	Al	V, Cr, Ni	250; 400
30	Pd-thick	Cu, Zn, U	1200; 1300
50	Cu	Mo	100; 200

^a Currents should be adjusted to the matrix that is measured (typically to maintain a dead time of ~30%).

calculating relative standard deviations (RSD's) of 2–4 replicate measurements, which express the standard deviation as percentage of the mean. Accuracy was determined by calculation of the coefficient of determination (R^2) of cross-plots of reference concentrations versus XCS intensity rates.

Direct comparison of intensities and concentrations provide fast and convenient information of the optimal count statistics for the XCS records, even when reference values are missing or below detection limits. However, bias in XCS intensity records by down-core changes of physical properties, measurement geometry, and non-linear matrix effects are best accommodated by the MLC model (Weltje et al., 2015). The MLC was performed using the AvaaXelerate software (Bloemsmas, 2015). The automated calibration sample selection option in the software was used to select a first subset of 32 samples for calibration. Extra samples were added to better cover the variability in our target elements. This resulted in a subset of 45 and 42 samples for, respectively, the wet and dry XCS measurements. For Mo the subset was smaller (23 and 22 samples, respectively) as samples with Mo concentrations below the detection limit of the ICP-OES measurements were excluded. Moreover, U was measured by ICP-MS in a lower resolution only, and hence the calibration subset existed of 23 samples for both wet and dry

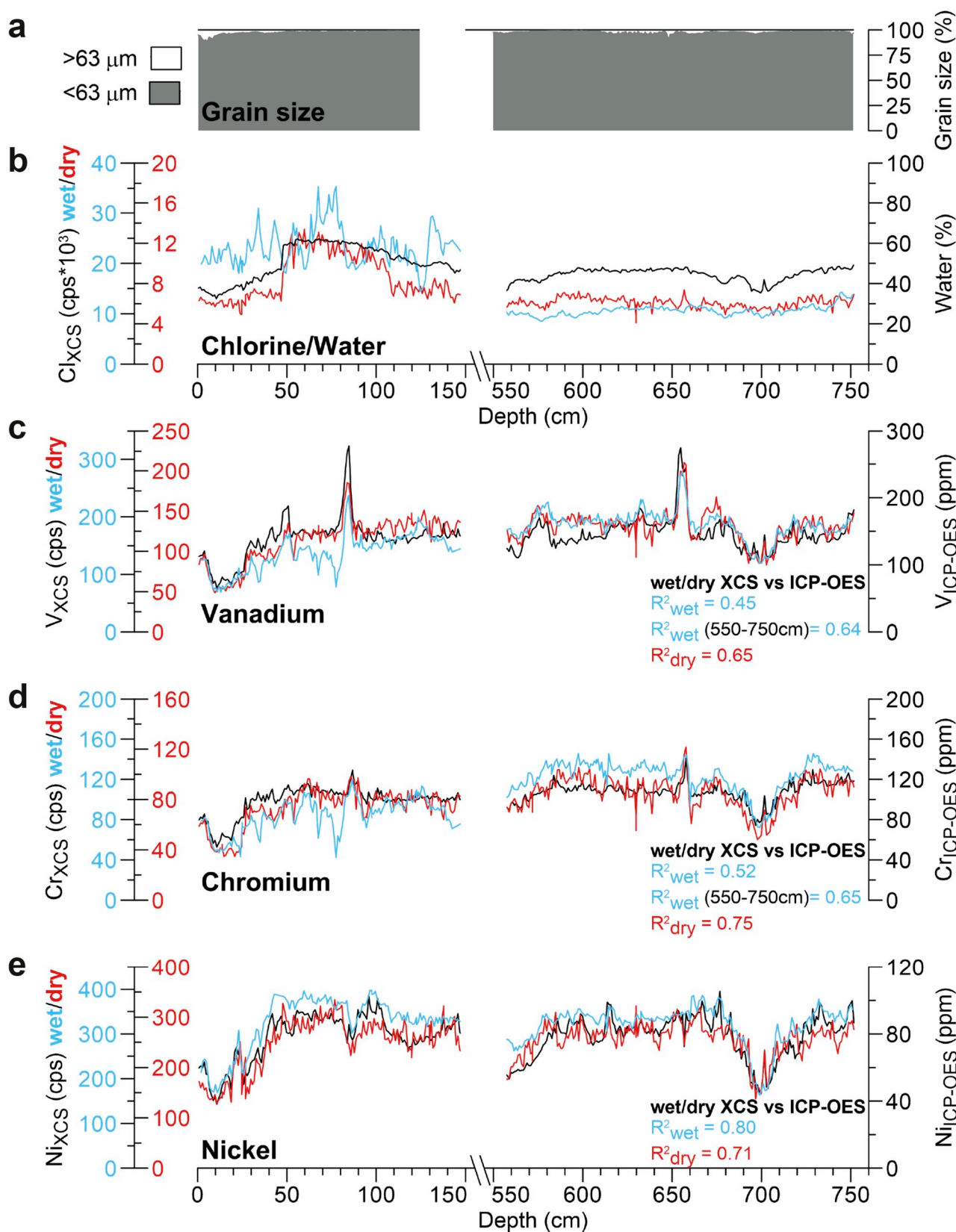


Fig. 4. (a) Grain size content (weight % of dry fraction) for core MS21 showing data for particles larger (white) and smaller (grey) than 63 μm . (b) The water content of the MS21 sediment (black), and the Cl intensities measured through XCS for wet (blue) and dry (red) MS21 samples. (c–i) Trace metal records for eastern Mediterranean core MS21 on a depth scale. Shown are: V (c), Cr (d), Ni (e), Cu (f), Zn (g), Mo (h), and U (i). The XCS measurements done on the wet core (blue) and dry sediment samples (red) are shown. Black lines indicate measurements done through ICP-OES, while for Mo and U also ICP-MS measurements are shown with black circles. Correlations between the ICP-OES and/or ICP-MS data with the wet XCS (blue) and dry XCS (red) are shown. (For interpretation of the references to color in this figure legend, the reader is referred to the Web version of this article.)

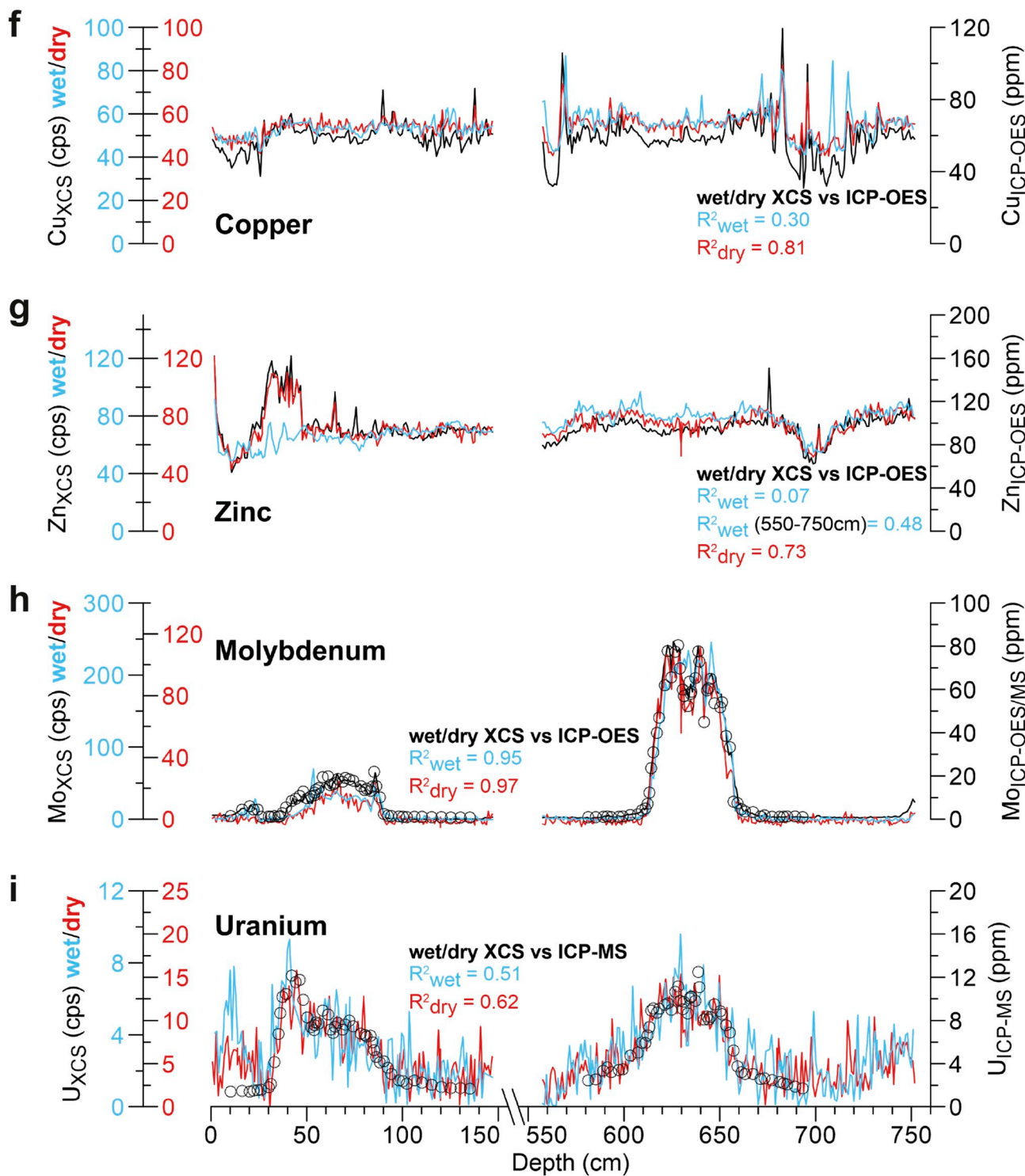


Fig. 4. (continued)

XCS measurements. These calibration samples were subsequently used with the MLC method in AavaXelerate to convert all XCS-derived trace metal intensities into concentrations. The accuracy and precision of the MLC method was then assessed using R^2 values of cross-plots of the XCS concentrations to the reference concentrations, and calculation of the RSD's from replicate XCS analyses, respectively.

2.5. Artificially produced laminated sediments

Synthetic V and Mo laminations in a calcite matrix were used to

assess whether XCS properly reflects sub-mm-scale variability for elements with highly contrasting XRF penetration depths. The synthetic laminations were produced by (1) resin-embedding a spiked calcite sample, (2) micro drilling grooves in this resin sample, and (3) filling up the grooves with another spiked calcite mixture and resin-embedding it again (Hennekam et al., 2015). These laminations with alternating V and Mo concentrations of ~40 ppm to ~400 ppm were subsequently measured every 0.1 mm using the previously established “optimal settings” (Section 3.1) and a slit size of 0.2 mm (down core) x 7 mm (cross core). A down-core slit size of 0.2 mm was used, because this was the

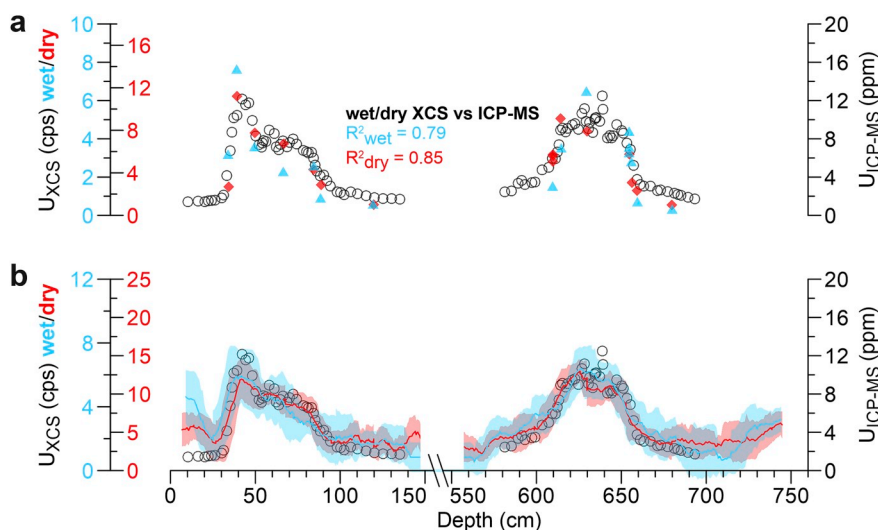


Fig. 5. (a) Profile of U in core MS21. The XCS measurement was performed with a 900s measurement time at 30 kV, with a Pd-Thick filter. The XCS measurements done on the wet core (blue) and dry sediment samples (red) are shown. Black circles indicate measurements done through ICP-MS. (b) Similar to Fig. 4i, but with a 15-point moving average for the wet and dry XCS measurements. The shading indicates the 15-point moving average standard deviation. (For interpretation of the references to color in this figure legend, the reader is referred to the Web version of this article.)

narrowest slit size where the signal-to-noise ratio of the obtained XRF spectra were adequate.

2.6. Matrix effects on trace metals with contrasting weights (V and Mo)

Polyethylene containers filled with pure calcite, quartz, and clay (montmorillonite) matrices spiked with V_2O_5 and MoS_2 were used to evaluate potential matrix effects on V and Mo intensities. Within these three matrices, ten different V and Mo concentrations were set, covering an approximate 0–2000 ppm range (see Hennekam et al., 2015). These mixtures were also analyzed by ICP-OES, ICP-MS, and XRF on glass beads (Hennekam et al., 2015). The averages of these three conventional methods were subsequently used as “reference” value for comparison to the XCS measurements. These XCS analyses were performed with the established “optimal settings” (Section 3.1) and a slit size of 10 mm (down core) x 10 mm (cross core).

3. Results and discussion

3.1. Optimal XCS method assessment for trace metal analysis

To assess the optimal XCS method, we first applied different energy settings (10–50 kV; in 5 kV steps) and different filters (no filter, Al-, Pd-thin-, Pd-thick-, and Cu-filter) on 14 eastern Mediterranean sediment samples and 8 standard samples that were dry, ground, and homogenized. For the different XCS settings we observed variable R^2 values for the trace metals V, Cr, Ni, Cu, Zn, Mo, and U analyzed in the 14 eastern Mediterranean sediment samples (Table 1). High R^2 values for V and Zn, generally exceeding 0.70, show that these two elements can be measured accurately over a wide range of settings. The elements Cr, Ni, and Cu, show moderate R^2 values, in the range of 0.40–0.50 (Table 1), for the sediments from the Mediterranean Sea. However, when including standard samples covering a larger concentration range (Cr: 10–137 ppm, Ni: 7–104 ppm, Cu: 13–426 ppm) R^2 values exceed 0.80 for Cr, Ni, and Cu for some settings (Table 1). Results for Mo show high R^2 values, exceeding 0.85 for most settings between 30 and 50 kV energies with Pd-thick- and Cu-filters applied (Table 1). For U, on the other hand, R^2 values rarely exceed 0.40 (Table 1). Possibly this lack of a close fit between off-line and XCS data is related to counting of U on the L-emission lines, while the other trace metals are measured at their K-lines. This suggests that increasing the measurement times for U would improve the analytical performance (i.e., the signal-to-noise ratio of U in the XRF spectra). Based on these first tests, 19 settings were selected to evaluate precision and optimal counting times for the XCS measurements (blue highlighted settings in the left column of Table 1).

These settings were mainly focused on (1) 10–30 kV without filter and with Al and Pd-thin filters for V, Cr, Ni, Cu, and Zn, and (2) 30–50 kV with Pd-thick and Cu filters for Mo and U.

The five best settings for each element, based on highest R^2 values, are highlighted in Fig. 1. For all of the five settings, precision and accuracy to determine V is high (RSD < 10%; $R^2 \geq 0.85$; Fig. 1a). For Cr, R^2 values based on the eastern Mediterranean samples alone are lower ($R^2 \geq 0.50$; Fig. 1b), which likely reflects the narrow concentration range of these samples (97–127 ppm). The R^2 values are much higher for Cr when the standards are included (10–137 ppm; $R^2 \geq 0.90$). The precision for Cr, as indicated by the RSD's, are between 2 and 15% for most settings. Results for Ni, Cu, and Zn show that a high precision (< 5%) is achievable for all these elements, as well as a high accuracy, especially as a wider concentration range is measured (Fig. 1c, d, e). Results for Mo showed some high RSD's, which likely reflect the samples below the detection limit (e.g., 5 ppm; Fig. 2). However, typically, precision for Mo is better than 20% for concentrations ≥ 10 ppm (Fig. 1f; samples below < 10 ppm were excluded here), and high accuracy is achievable ($R^2 \geq 0.90$; Fig. 1f). The precision for U is generally better than 30%, while the R^2 values clearly increase with analytical dwell time for U, being higher than 0.5 if dwell times exceed 30 s (Fig. 1g). The R^2 values for U reach a maximum of approximately 0.80 for the Mediterranean samples and approximately 0.65 when the standards are included (Fig. 1g). The lower R^2 values for the samples including the standards, relative to those without the standards, may result from the variable composition of the standards causing additional deviations related to matrix effects on U.

The highest accuracy/precision for trace metals V, Cr, Ni, Cu, Zn, Mo, and U are achieved using: (1) V and Ni at energies between 15 and 30 kV with an Al filter, (2) Cr at energies between 20 and 30 kV with an Al filter, (3) Cu, Zn, and U at energies between 30 and 45 kV with a Pd-thick filter, and (4) Mo at energies between 30 and 50 kV with a Cu filter. The RSD's and R^2 values show that an appropriate measurement time for trace metals V, Cr, Ni, Cu, Zn, Mo is ≥ 30 s, while the measurement time for U should be as high as possible (here a maximum 120s was used). Clearly, all these trace elements benefit from background reduction using a primary beam filter, which is placed between the X-ray tube and the sample. Background reduction using these filters has been common practice for trace-element analysis in conventional XRF analyses (Gedcke et al., 1977; Potts et al., 1984). For XCS the signal-to-noise (peak height to background) also increases when these filters are applied (see Fig. 3 for examples of spectra from 20, 30, and 50 kV), which significantly improves trace metal analyses.

Several settings show high precision and accuracy for the target elements, but for practical considerations (i.e., highest time efficiency),

three settings are selected here for further evaluation (Table 2). The setting at 20 kV with an Al filter allows precise/accurate analyses of V, Cr, and Ni. Moreover, high precision/accuracy is obtained for Cu, Zn, and U at 30 kV with a Pd-thick filter. Lastly, precise/accurate analysis of Mo is obtained at 50 kV with a Cu filter. The latter setting has an additional advantage that it allows the detection of barium (Ba), which is often analyzed in the context of changes in export productivity (e.g., Van Santvoort et al., 1997). Hence, with these three XCS settings a suite of trace elements is covered which are often considered relevant in the context of paleoceanographic studies. These will therefore be considered “optimal” settings for subsequent analyses on a core from the

eastern Mediterranean Sea (Table 2). All these subsequent analyses were performed using a 60 s count time, except for the wet-XCS analysis of U (120 s). These optimal settings are almost identical to those achieved using the previous generation Canberra detector on samples covering a larger concentration range (Supplementary Material), indicating that these settings are probably inherent to the method and not the detector as such.

3.2. Eastern Mediterranean Sea sediment record

To test our optimized XCS settings for trace-metal analyses, we

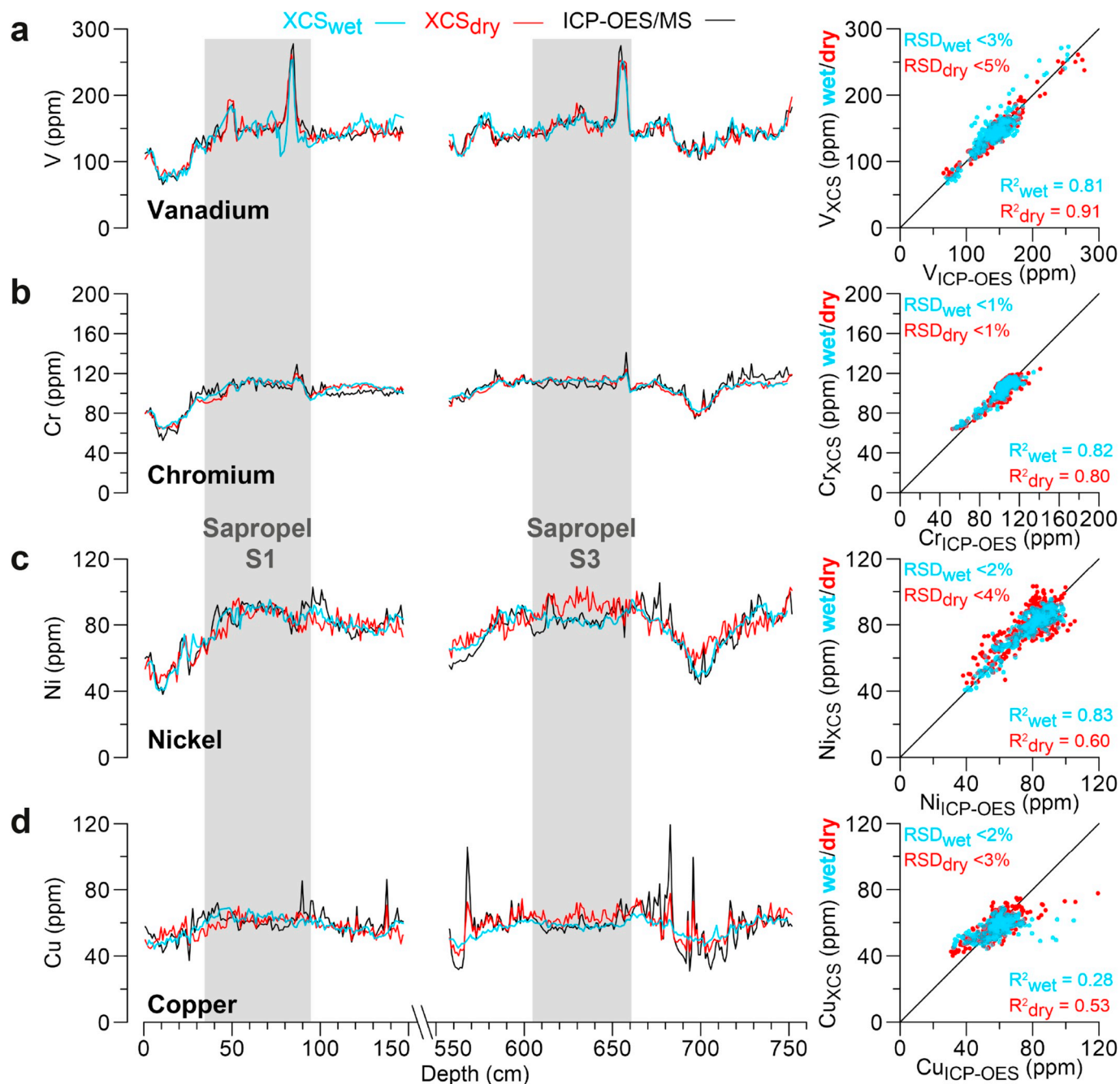


Fig. 6. Trace metal concentration records for eastern Mediterranean core MS21 on a depth scale. Shown are: V (a), Cr (b), Ni (c), Cu (d), Zn (e), Mo (f), and U (g). The XCS intensities, performed on the wet core (blue) and dry sediment samples (red), were converted into concentrations using the MLC approach (Weltje et al., 2015; see Section 2.4). Black lines indicate measurements done through ICP-OES or ICP-MS (for U). The grey areas indicate the positions of Mediterranean sapropels S1 and S3. The right panels show X-Y plots of XCS concentrations (wet XCS in blue and dry XCS in red) versus the ICP-OES/ICP-MS data with their coefficient of determination (R^2). The RSD of replicate measurements are also indicated. (For interpretation of the references to color in this figure legend, the reader is referred to the Web version of this article.)

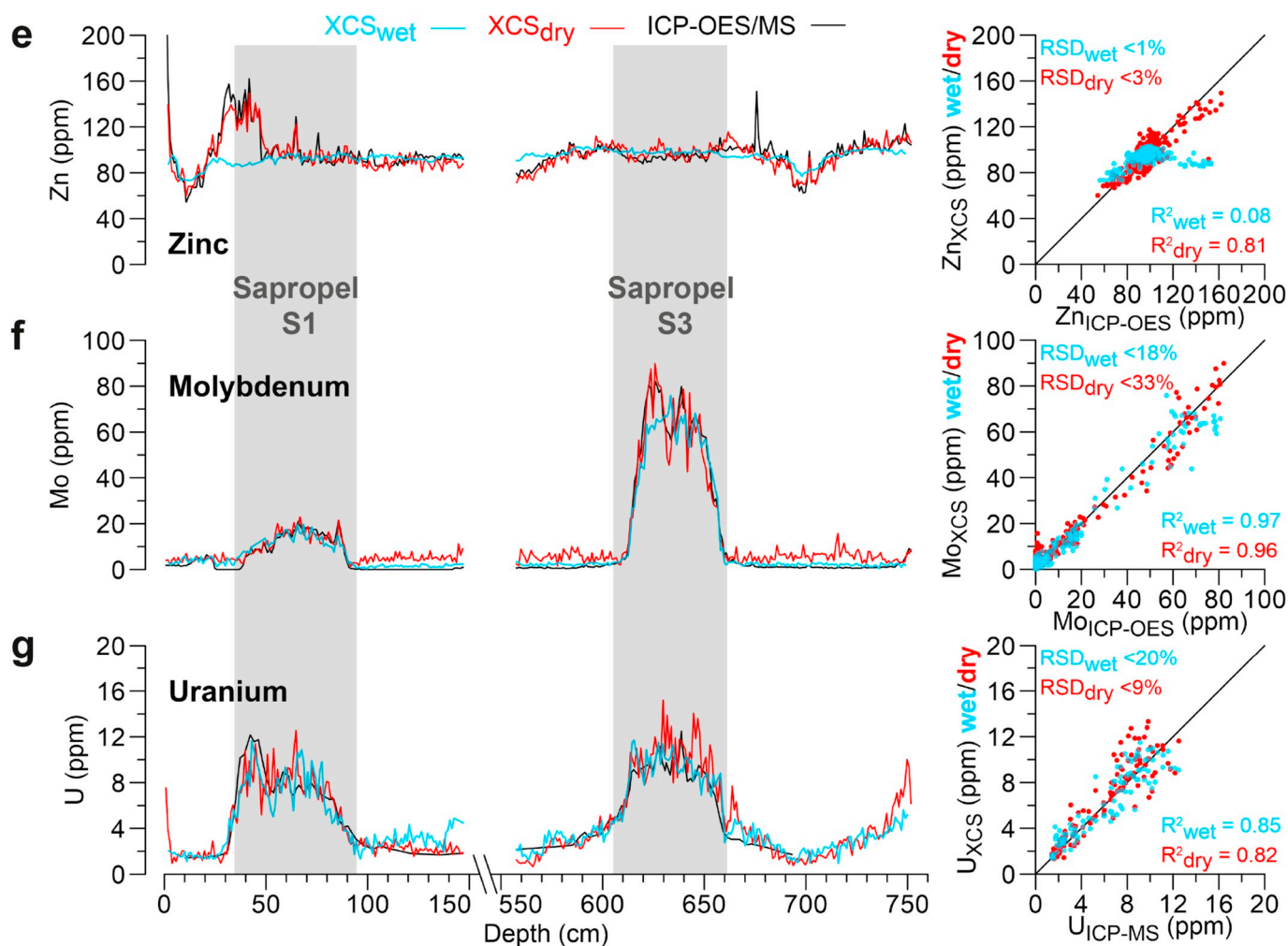


Fig. 6. (continued)

measured sediment cores from the eastern Mediterranean Sea with known trace-metal distribution. The intervals shown here contain two periods of sustained anoxic conditions at 35–95 cm (Sapropel S1) and 605–660 cm (Sapropel S3). These events are also characterized by elevated concentrations of trace metals often associated with bottom water anoxia (Nijenhuis et al., 1999; Passier et al., 1999; Warning and Brumsack, 2000; Zwiép et al., 2018). The sediments consist for $\geq 90\%$ of clay/silt ($< 63 \mu\text{m}$ grains; Fig. 4a), being excellently suited for XCS analyses (Richter et al., 2006). The top sections of the core contain high amounts of interstitial water, with the wettest part containing 60–65 weight % water, while the lower sections are relatively dry with values between 40 and 50 weight % of water (Fig. 4b). The dry-XCS measurements of chlorine (Cl) closely follow the water content, while the Cl intensity rates analyzed on the wet core section show much larger deviations, especially in the top sections. This most likely reflects (random) pooling of water under the foil used during the XCS analyses (Kido et al., 2006; Tjallingii et al., 2007; Hennekam and De Lange, 2012), which may potentially also affect trace-metal analyses by XCS.

Fig. 4c–i shows the trace-metal composition measured with dry/wet XCS versus ICP-OES/ICP-MS analyses, including R^2 values comparing the XCS analyses with these reference values. Absorption effects of a water film under the foil may be recognized in the V and Cr intensities. This is shown by a dip in wet-XCS intensities at 60–80 cm (Fig. 4c and d) corresponding with a peak in Cl intensities in the wet core (Fig. 4b). Moreover, V and Cr show lower R^2 values for the wet-XCS measurements relative to the measurements done on dry sediment. The other trace metals do not show similar dips, which probably reflects their

higher atomic number and hence higher fluorescence energies, which are less easily absorbed (e.g., Tjallingii et al., 2007). Nonetheless, in sediment with interstitial water contents between 40 and 50% (550–750 cm), such effects are no longer apparent for V and Cr, with R^2 values being much more similar for wet and dry measurements (Fig. 4c and d).

The trace metal data measured by wet and dry XCS show reasonable to high correlations to the conventional analyses on discrete samples (Fig. 4c–i). The dry XCS measurements show, generally, the highest correlation to ICP-OES/ICP-MS data. Apart from water film effects, this is likely due to the dry XCS measurements being performed on exactly the same samples as the conventional measurements. The wet XCS measurements may potentially be slightly offset in the depth domain compared to the discrete samples, thereby adding to the uncertainty. Moreover, the core-based XCS analyses were not performed on homogenized powders, which is another source of potential bias. As such, deviations in XCS results for Cu and Zn relative to ICP-OES values may largely be due to small-scale inhomogeneity in the wet sediment surface compared to the ground sediment samples (Fig. 4f and g).

The down-core U concentration profile captures the large-scale trend, as also revealed by ICP-MS measurements, albeit with appreciable more scatter (Fig. 4i). Longer dwell times clearly improve the XCS analyses (Section 3.1), as also suggested by measurements done with analysis times of 900 s (Fig. 5a). Similarly, several measurements can be condensed into a single data point by calculating of a 15-point moving average (Fig. 5b). This shows that the U profiles closely matches the ICP-MS-based concentration trend. The noise in the XCS-based U record

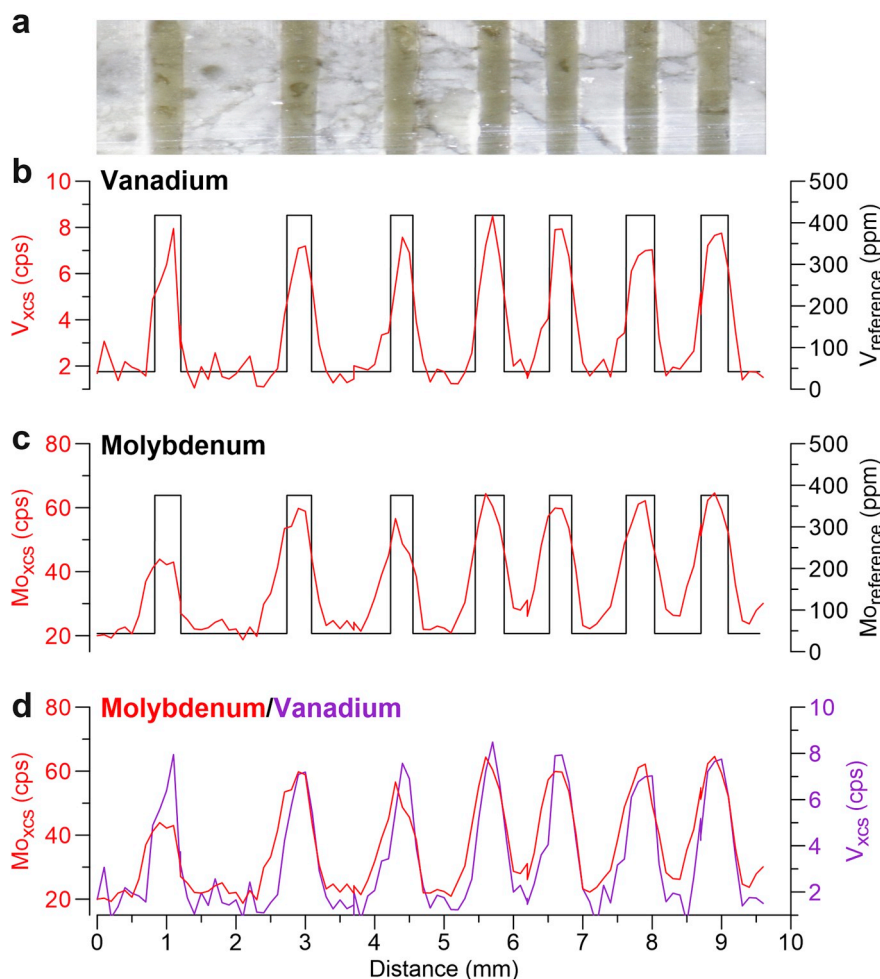


Fig. 7. Artificially produced, laminated sediment containing variable concentrations of trace metals with contrasting atomic weights (V and Mo) in a calcite matrix. (a) Picture of the synthetic laminations. (b) XCS measurement of V (red) compared to the reference concentration (black) over a line-scan profile of ~1 cm (c) XCS measurement of Mo (red) compared to the reference concentration (black) over a line-scan profile of ~1 cm. (d) Direct comparison of line-scan profiles of Mo (red) and V (purple) measured through XCS. (For interpretation of the references to color in this figure legend, the reader is referred to the Web version of this article.)

likely primarily reflects the relatively low sedimentary concentrations (maximum: ~13 ppm; average: ~6 ppm). Nonetheless, U is an important indicator for sub-oxic conditions (e.g., Tribovillard et al., 2012), and even though these records contain some scatter, they yield important information on initiation/termination of sub-oxic sedimentary conditions.

The results for the elements investigated here show that measuring sedimentary trace-metal content using XCS is feasible. Larger variability in the trace metals, such as present in black shales (Brumsack, 2006), likely result in much higher R^2 values. This is exemplified by the results for Mo (Fig. 4h), showing a strong increase during the sapropels, relative to the background values, which results in R^2 values of ≥ 0.95 for both wet and dry XCS analyses. As such, our results show that time- and cost-efficient trace metal data can now be acquired from many depositional environments using XCS, provided that other parameters that affect XCS analyses (e.g., matrix, grain size) remain relatively constant. These data become especially useful when converted into quantitative concentrations.

The MLC algorithm provides a state-of-the-art approach for calibration of XCS analyses (Weltje et al., 2015), which we applied to our XCS intensity data (Fig. 6). Most trace metal concentrations derived by XCS show strong correlation with the concentrations of conventional methods (Fig. 6a–g), except for the elements that already strongly deviated as intensity data (e.g., inhomogeneity impact on wet-XCS Cu data). Overall, the elements V, Cr, Ni, Mo, and U show reasonable to

high precision/accuracy (Fig. 6a, b, c, f, g), while for Ni and Cu this is achieved predominantly for the dry XCS data (Fig. 6d and e). For sedimentary records, especially when somewhat drier (< 50 weight % water), the MLC approach thus allows fast establishing quantitative trace-metal data, requiring only a minimum amount (~30–40 samples) of conventional data to be generated for calibration purposes. These quantitative trace-metal data are highly complementary to other major and minor elemental data, which can be used to reconstruct past bottom-water anoxia and organic-matter deposition, such as Br (marine organic carbon), Ba (export productivity), Mn (redox transitions through manganese oxides), Fe (pyrites versus iron-oxides), and S (pyrites and other sulfides) (Van Santvoort et al., 1997; Ziegler et al., 2008; Croudace and Rothwell, 2015).

3.3. High-resolution, sub-mm profiles for trace metals with contrasting atomic weights

The XCS analysis of synthetic laminations shows the capability of XCS to capture sub-mm variability in two trace metals (V and Mo) with highly deviating fluorescence energies and potential effects of different penetration depths (Fig. 7). The laminae are well recognizable in the XCS data for both V and Mo, and generally the XCS profiles closely follow the reference data. However, the transitions between two consecutive layers is smoother in the XCS data, compared to the abrupt transition in the reference data. This is likely related to the irradiated

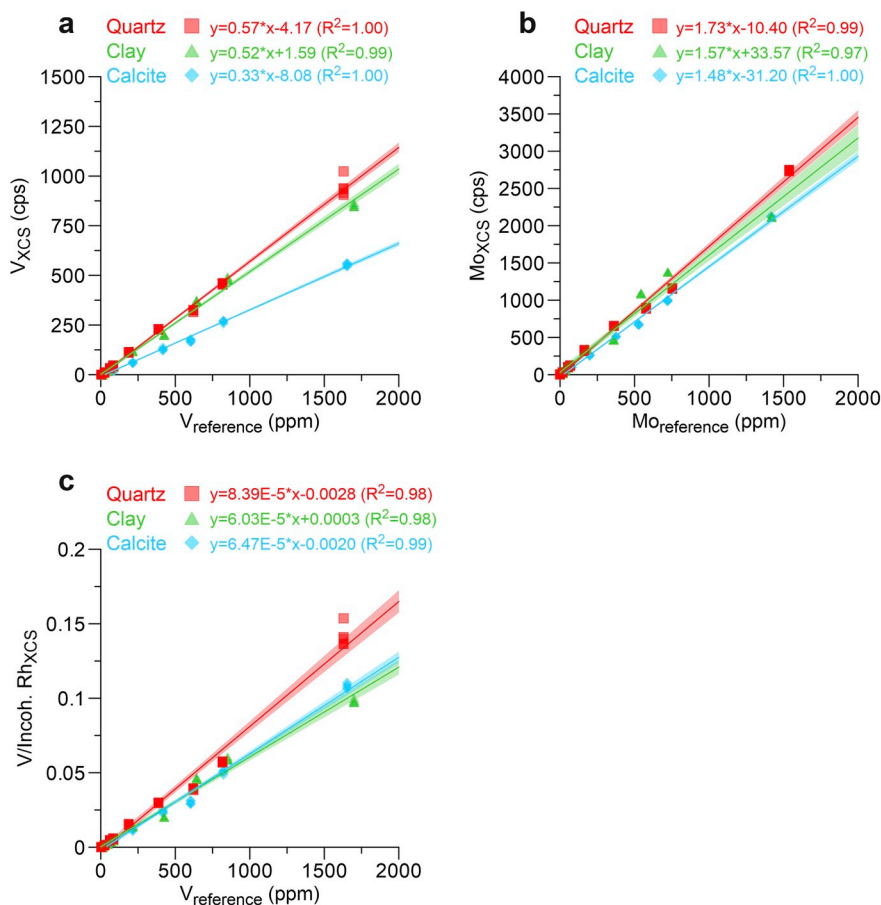


Fig. 8. (a) Concentration versus XCS intensity plot for V, with correlations given at the top. (b) Concentration versus XCS intensity plot for Mo. (c) Reference concentrations versus V to Rh incoherent radiation intensity ratios. In all plots the matrices of quartz (red squares), clay (green triangles), and calcite (blue diamonds) are shown. The shadings indicate the 99% confidence intervals of the linear regressions. (For interpretation of the references to color in this figure legend, the reader is referred to the Web version of this article.)

surface area of 0.2×7 mm, which is large compared to the sharp transitions, and probably also to the penetration depth and related excited volume (“balloon effect”) from which the XRF signal originates (Potts et al., 1997). The higher energy X-rays of Mo, relative to V, originate from deeper depths, causing a smoother transition for Mo in comparison to V. This is especially apparent at 5–10 mm when the laminations are closer together (Fig. 7d). In geological samples, approximately 90% of the signal comes from 20 to 30 μ m depth for V, while for Mo this is in the order of 600–800 μ m depth (Potts et al., 1997). As such, in fine sequences of laminae this may result in somewhat smoothing of signals of heavier elements, but generally sub-mm signals are measured well through XCS. Here, this is exemplified by the elements V and Mo (selected for their contrasting atomic masses), but these results likely also apply to other (trace) elements, presuming that these were measured with good signal-to-noise ratio in the spectra.

3.4. Matrix effects for V in quartz, clay, and calcite samples

We performed XCS analyses on prepared mixtures of common, pure sediment matrices (quartz, clay, calcite) with increasing concentrations of V and Mo to evaluate potential matrix effects on V and Mo intensities (Fig. 8a–b). As sample geometry can be considered equal for all these samples, differences are attributed to differences in matrix. In general, within all matrices, regressions are obtained with high R^2 values of ≥ 0.97 . However, it is clear that for V in the calcite matrix, the slope is lower than that observed for quartz or clay (Fig. 8a), while for Mo the slopes are much more similar between the different matrices (Fig. 8b). The different slopes for V likely reflects differences in absorption, which depends on the concentration of the other elements in the matrix (i.e., matrix effects). Calcium (Ca) in calcite is known as an efficient absorber of V fluorescence radiation, as the K-line energies of the V photons lie just above the absorption edge of Ca (Potts, 1987). Hence, this shows

that for sediments with a large variability in Ca, which often occurs in the marine environment, correction for these matrix effects might be necessary to properly analyze sedimentary V by XCS.

A simple way to reduce matrix effects in XRF is by normalization to incoherent (Compton) radiation (e.g., Nesbitt et al., 1976; Croudace and Gilligan, 1990). Matrix absorption may affect trace-metal fluorescence radiation similarly as incoherent scattering of the Rh X-Ray tube radiation (Croudace and Gilligan, 1990). The results improve for the calcite and clay matrices when comparing reference concentrations to V/Rh_{incoherent} ratios instead of V intensities (Fig. 8c). However, the slope of the mixtures in a quartz matrix is deviating when this correction is applied. This might be attributed to the non-linear nature of absorption effects that become more apparent when a wider range of concentrations is regarded (Croudace and Gilligan, 1990; Weltje and Tjallingii, 2008). This means that non-linear matrix effects can strongly change depending on the sediment composition. Correcting of the Ca matrix effects on V using the incoherent scattering may thus be reasonable, but only when concentration differences in V and matrix are limited.

4. Conclusions

Sedimentary trace elements are useful indicators to study, e.g., water-column oxygenation, productivity, sediment provenance, and environmental pollution. We show that, in addition to major and minor elements, XCS can now be used to extract information about sedimentary trace-metal (V, Cr, Ni, Cu, Zn, Mo, and U) contents from core material, much faster than traditional techniques. The XCS data show that general trends and variability in trace metals are well-captured (depending on concentration ranges), even for sub-mm resolutions.

Three optimal settings to analyze sediments for our target trace metals arise from our detailed exploration: 20 kV with Al primary beam

filter (V, Cr, Ni), 30 kV with Pd-thick primary beam filter (Cu, Zn, U), and 50 kV with Cu primary beam filter (Mo). For individual trace metals (Cr, Ni, Cu, and Zn) other settings may result in slightly better precision/accuracy, but these three settings cover the whole suite of trace metals while limiting the analytical time. For major element analysis, a 10 kV run (no filter) can be added, which would warrant a good coverage of the entire range of elements measurable through XCS. Generally, measurements of ≥ 30 s are required to obtain reliable data for trace metals through XCS. The obtained semi-quantitative measurements can be calibrated using low-resolution geochemical data from conventional methods, by application of a multivariate log-ratio calibration approach, which yields good estimates of trace metal concentrations in both wet and dry sediment samples.

The quantitative measurement of trace elements by XCS opens a wide array of new possibilities to produce long-term (paleo-)records on water-column dynamics (particulate shuttling), seafloor anoxia, organic carbon burial, sediment provenance, environmental pollution, and many other environmental parameters.

Acknowledgements

We acknowledge the constructive comments by two anonymous reviewers, which were helpful to improve the original manuscript. This research is made possible by financial support to the MEDIFLUX-project (855.01.031) and related MIMES cruise, the PALM-project (820.01.005), and the SCANALOGUE-project (ALWOP.2015.113) by the Netherlands Organisation for Scientific Research (NWO). This study was also partially carried out under the program of the Netherlands Earth System Science Centre, financially supported by the Dutch Ministry of Education, Culture and Science (OCW). We thank Erik van Vilsteren (ICP-MS), Helen de Waard (ICP-MS), and Ton Zalm (ICP-OES) for analytical assistance at the Utrecht University, and captain, crew, and scientific team of MIMES cruise for core recovery. Sander van den Boorn of Shell Global Solutions Int. kindly provided access to the Jordan core material and XRF-core-scan data, which is used in the Supplementary Material.

Appendix A. Supplementary data

Supplementary data to this article can be found online at <https://doi.org/10.1016/j.quaint.2018.10.018>.

References

- Algeo, T.J., Lyons, T.W., 2006. Mo-total organic carbon covariation in modern anoxic marine environments: implications for analysis of paleoredox and paleohydrographic conditions. *Paleoceanography* 21.
- Algeo, T.J., Rowe, H., 2012. Paleoceanographic applications of trace-metal concentration data. *Chem. Geol.* 324–325, 6–18.
- Algeo, T.J., Tribouillard, N., 2009. Environmental analysis of paleoceanographic systems based on molybdenum-uranium covariation. *Chem. Geol.* 268, 211–225.
- Bloemsma, M.R., 2015. Development of a Modelling Framework for Core Data Integration Using XRF Scanning. Ph.D. thesis. Delft University of Technology, The Netherlands, pp. 229 pp.
- Bruland, K.W., 1980. Oceanographic distributions of cadmium, zinc, nickel, and copper in the North Pacific. *Earth Planet Sci. Lett.* 47, 176–198.
- Brumsack, H.-J., 2006. The trace metal content of recent organic carbon-rich sediments: implications for Cretaceous black shale formation. *Palaeogeogr. Palaeoclimatol. Palaeoecol.* 232, 344–361.
- Croudace, I.W., Gilligan, J.M., 1990. Versatile and accurate trace element determinations in iron-rich and other geological samples using x-ray fluorescence analysis. *X Ray Spectrom.* 19, 117–123.
- Croudace, I.W., Rothwell, R.G., 2015. *Micro-XRF Studies of Sediment Cores: Applications of a Non-destructive Tool for the Environmental Sciences*. Springer Science + Business Media, Dordrecht.
- Garver, J.I., Royce, P.R., Smick, T.A., 1996. Chromium and nickel in shale of the Taconic foreland: a case study for the provenance of fine-grained sediments with an ultramafic source. *J. Sediment. Res.* 66, 100–106.
- Gedcke, D., Elad, E., Denee, P., 1977. An intercomparison of trace element excitation methods for energy-dispersive fluorescence analyzers. *X Ray Spectrom.* 6, 21–29.
- Gibson, K.A., Peterson, L.C., 2014. A 0.6 million year record of millennial-scale climate variability in the tropics. *Geophys. Res. Lett.* 41, 969–975.
- Hennekam, R., De Lange, G.J., 2012. X-ray fluorescence core scanning of wet marine sediments: methods to improve quality and reproducibility of high-resolution paleoenvironmental records. *Limnol. Oceanogr. Methods* 10, 991–1003.
- Hennekam, R., Jilbert, T., Mason, P.R.D., de Lange, G.J., Reichart, G.-J., 2015. High-resolution line-scan analysis of resin-embedded sediments using laser ablation-inductively coupled plasma-mass spectrometry (LA-ICP-MS). *Chem. Geol.* 403, 42–51.
- Jarvis, S., Croudace, I.W., Rothwell, R.G., 2015. Parameter optimisation for the ITRAX core scanner. In: Croudace, I.W., Rothwell, R.G. (Eds.), *Micro-XRF Studies of Sediment Cores*. Springer Science + Business Media, Dordrecht, pp. 535–562.
- Kido, Y., Koshikawa, T., Tada, R., 2006. Rapid and quantitative major element analysis method for wet fine-grained sediments using an XRF microscanner. *Mar. Geol.* 229, 209–225.
- Nesbitt, R., Mastins, H., Stolz, G., Bruce, D., 1976. Matrix corrections in trace-element analysis by X-ray fluorescence: an extension of the Compton scattering technique to long wavelengths. *Chem. Geol.* 18, 203–213.
- Nijenhuis, I.A., Bosch, H.J., Sinnighe Damsté, J.S., Brumsack, H.J., De Lange, G.J., 1999. Organic matter and trace element rich sapropels and black shales: a geochemical comparison. *Earth Planet Sci. Lett.* 169, 277–290.
- Passier, H.F., Bosch, H.-J., Nijenhuis, I.A., Lourens, L.J., Bottcher, M.E., Leenders, A., Sinnighe Damsté, J.S., de Lange, G.J., Leeuw, J.W., 1999. Sulphidic Mediterranean surface waters during Pliocene sapropel formation. *Nature* 397, 146–149.
- Potts, P., Webb, P., Watson, J., 1984. Energy-dispersive x-ray fluorescence analysis of silicate rocks for major and trace elements. *X Ray Spectrom.* 13, 2–15.
- Potts, P.J., 1987. *A Handbook of Silicate Rock Analysis*. Blackie, Glasgow and London 622 pp.
- Potts, P.J., Williams-Thorpe, O., Webb, P.C., 1997. The bulk analysis of silicate rocks by portable X-ray fluorescence: effect of sample mineralogy in relation to the size of the excited volume. *Geostand. Geoanal. Res.* 21, 29–41.
- Richter, T.O., van der Gaast, S., Koster, B., Vaars, A., Gieles, R., de Stigter, H.C., de Haas, H., van Weering, T.C.E., 2006. The Avaatech XRF Core Scanner: technical description and applications to NE Atlantic sediments. In: Rothwell, R.G. (Ed.), *New Techniques in Sediment Core Analysis*. Special Publications. Geological Society, London, pp. 39–50.
- Rohling, E., Marino, G., Grant, K., 2015. Mediterranean climate and oceanography, and the periodic development of anoxic events (sapropels). *Earth Sci. Rev.* 143, 62–97.
- Rohling, E.J., Hibbert, F.D., Williams, F.H., Grant, K.M., Marino, G., Foster, G.L., Hennekam, R., De Lange, G.J., Roberts, A.P., Yu, J., 2017. Differences between the last two glacial maxima and implications for ice-sheet, $\delta^{18}\text{O}$, and sea-level reconstructions. *Quat. Sci. Rev.* 176, 1–28.
- Ruiz, F., 2001. Trace metals in estuarine sediments from the southwestern Spanish coast. *Mar. Pollut. Bull.* 42, 481–489.
- Sweere, T., van den Boorn, S., Dickson, A.J., Reichart, G.-J., 2016. Definition of new trace-metal proxies for the controls on organic matter enrichment in marine sediments based on Mn, Co, Mo and Cd concentrations. *Chem. Geol.* 441, 235–245.
- Tjallingii, R., Röhl, U., Kölling, M., Bickert, T., 2007. Influence of the water content on X-ray fluorescence core-scanning measurements in soft marine sediments. *G-cubed* 8 Q002004.
- Tribouillard, N., Algeo, T.J., Lyons, T., Riboulleau, A., 2006. Trace metals as paleoredox and paleoproductivity proxies: an update. *Chem. Geol.* 232, 12–32.
- Tribouillard, N., Algeo, T.J., Baudin, F., Riboulleau, A., 2012. Analysis of marine environmental conditions based on molybdenum-uranium covariation—applications to Mesozoic paleoceanography. *Chem. Geol.* 324–325, 46–58.
- Van Santvoort, P.J.M., De Lange, G.J., Langereis, C.G., Dekkers, M.J., Paterne, M., 1997. Geochemical and paleomagnetic evidence for the occurrence of "missing" sapropels in eastern Mediterranean sediments. *Paleoceanography* 12, 773–786.
- Warning, B., Brumsack, H.J., 2000. Trace metal signatures of eastern Mediterranean sapropels. *Palaeogeogr. Palaeoclimatol. Palaeoecol.* 158, 293–309.
- Weltje, G.J., Tjallingii, R., 2008. Calibration of XRF core scanners for quantitative geochemical logging of sediment cores: theory and application. *Earth Planet Sci. Lett.* 274, 423–438.
- Weltje, G.J., Bloemsma, M., Tjallingii, R., Heslop, D., Röhl, U., Croudace, I.W., 2015. Prediction of geochemical composition from XRF core scanner data: a new multivariate approach including automatic selection of calibration samples and quantification of uncertainties. In: Croudace, I.W., Rothwell, R.G. (Eds.), *Micro-XRF Studies of Sediment Cores*. Springer Science + Business Media, Dordrecht, pp. 507–534.
- Wirth, S.B., Gilli, A., Niemann, H., Dahl, T.W., Ravasi, D., Sax, N., Hamann, Y., Peduzzi, R., Peduzzi, S., Tonolla, M., 2013. Combining sedimentological, trace metal (Mn, Mo) and molecular evidence for reconstructing past water-column redox conditions: the example of meromictic Lake Cadagno (Swiss Alps). *Geochem. Cosmochim. Acta* 120, 220–238.
- Yang, S.Y., Jung, H.S., Lim, D.I., Li, C.X., 2003. A review on the provenance discrimination of sediments in the Yellow Sea. *Earth Sci. Rev.* 63, 93–120.
- Ziegler, M., Jilbert, T., De Lange, G.J., Lourens, L.J., Reichart, G.-J., 2008. Bromine counts from XRF scanning as an estimate of the marine organic carbon content of sediment cores. *G-cubed* 9 Q05009.
- Zwief, K.L., Hennekam, R., Donders, T.H., van Helmond, N.A.G.M., de Lange, G.J., Sangiorgi, F., 2018. Marine productivity, water column processes and seafloor anoxia in relation to Nile discharge during sapropels S1 and S3. *Quat. Sci. Rev.* 200, 178–190.